Available online at www.sciencedirect.com
ScienceDirect
Optics Communications 281 (2008) 1293–1299
OPTICS COMMUNICATIONS
www.elsevier.com/locate/optcom

The plasmon and distribution effects between incident light and active layer in PtO_x-type super-resolution near-field structure

Yuan-Fong Chau [a,*], Din Ping Tsai [b], Lin-Fang Shen [c], Tzong-Jer Yang [d], Yuh-Sien Sun [a]

[a] Department of Electronic Engineering, Ching Yun University, Jung Li, Taiwan, ROC
[b] Department of Physics and Center for Nanostorage Research, National Taiwan University, Taipei, Taiwan, ROC
[c] Department of Information Science and Electronic Engineering, and Electromagnetic Academy, Zhejiang Province, Hang Zhou 310027, PR China
[d] Department of Electrophysics, National Chiao-Tung University, HsinChu 300, Taiwan, ROC

Received 1 May 2007; received in revised form 14 October 2007; accepted 22 October 2007

Abstract

The plasmon and distribution effects of collective localized surface plasmons between incident light and active layer of PtO_x-type super resolution near-field structure (super-RENS) have been studied using finite-difference time-domain method. Four types of distribution of Pt nanoparticles, i.e., type A, B, C, and D in active layer are investigated. We find that type C and D in active layer can provide higher field intensity in a wider range of particle size when the particle sizes are varied, and the out-going filed emerging from the active layer exhibit smaller spot size than those of type A and B. Type B, C and D also provide the additional path longer than that of type A, and excite more evanescent field which located in the far edge of the bubble from the optical axis of the incident beam. Results show that the type C structure is the best choice in the view point of designing the PtO_x-type super-RENS. This study provides new information to design a super-RENS with superior resolution as well as other applications in nano photonic devices.

PACS: 42.79.Vb; 71.15.Rn; 72.15.Rn; 73.22.−f; 73.22.Lp; 78.67.Bf; 73.20.Mf

The super-resolution near-field structure (super-RENS) [1–7] disc is a promising candidate for next-generation optical disc to achieve the high data storage capacity. Today, this novel emergent technique, near-field optical data storage, allows the writing and/or reading of information bits which are smaller than the resolution limit of the optical head without increasing the complexity of the detecting system. Such a technique is very attractive because of its compatibility with existing players/recorders. Near-field optical data storage techniques depend on the evanescent coupling of light to the data layer of the optical storage medium to read and write data marks that are smaller than the diffraction limit of conventional optical data storage systems. In recent years, there has been increased attention given to techniques that may overcome this limit. Among the various types of super-RENS disc, the third-generation super-RENS disc with a platinum oxide (PtO_x) layer has been shown several advantages in terms of readout characteristics and readout stability [8,9].

The PtO_x-type super-RENS disc is a write-once recording medium, and the recording pits are solidified by PtO_x decomposition [10,11]. A PtO_x-type super-RENS structure is composed of an active layer (PtO_x film) that is sandwiched between two dielectric films ($ZnS–SiO_2$), and this three-layer stack is deposited directly on the phase-change data layer ($Ge_2Sb_2Te_5$) of a disk. One of the dielectric layers is directly adjacent to a polycarbonate layer acting as an insulating layer; the other dielectric layer is the cover layer. If a storage medium incorporates a super-RENS, the light spot that probes the data layer is smaller than the size of the focused spot that is incident on the cover layer of the super-RENS structure. The optical aperture serves as a

* Corresponding author. Tel.: +886 3 4581196x5105; fax: +886 3 4581196.
E-mail address: yfc01@cyu.edu.tw (Y.-F. Chau).

0030-4018/$ - see front matter © 2007 Elsevier B.V. All rights reserved.
doi:10.1016/j.optcom.2007.10.072

probe on the disk like that for scanning near-field optical microscopy (SNOM). After recording on a phase-change layer, small marks are reproduced through the aperture. The particles, instead of the aperture, function as the scattering center, which is the key to inducing the super-resolution phenomenon. The 15–20 nm PtO_x thin films are considered to be nonlinear optical layers which control the near-field optical aperture. Recently, several studies have explored this nonlinear near-field optical property; [12–16]however, the influence of the deformed super-RENS structure does not seem to be appropriately considered. The active layer of the super-RENS structure is deformed after a writing process, as observed in experimental work [17,18] and the platinum (Pt) nanoparticles spread out in the bubble pit (deformed PtO_x film).

In order to examine this nonlinear near-field optical property and match it to a realistic situation, we study the relationships between the active layer (PtO_x bubble pit) and incident light for various diameters of Pt nanoparticles on the smooth and deformed active layer using finite-difference time-domain (FDTD) [19] method. Results indicate a close connection between the surface plasmon effects of Pt nanoparticles and the nonlinear near-field optical property observed in experiments.

1. Simulation models

Firstly, four types of active layer (PtO_x film) are illustrated for analysis, type A [normal (undeformed active layer), Pt nanoparticles distribute randomly in a flat active layer], type B [Pt nanoparticles distribute randomly inside a bubble pit (deformed active layer)], type C (Pt nanoparticles distribute in a square distribution inside the bubble pit), and type D (Pt nanoparticles distribute in a triangular distribution inside the bubble pit), as shown in Figs. 1a–d, respectively. For these four types, we assume that the Pt nanoparticles are of the same size. The layer structure is, from bottom to top, polycarbonate ($n = 1.5$)/ZnS–SiO_2 ($n = 2.25 + i0.01$)/PtO_x ($n = 3.2 + i1.6$)/ZnS-SiO_2/$Ge_2Sb_2Te_5$ (GST, crystal phase, $n_c = 4.01 + i3.61$)/ZnS–SiO_2/air ($n = 1$). Figs. 1b–d show that the layer structure between the insulating layer (the second ZnS–SiO_2) and the record mark (GST) are deformed after the writing process. The Pt nanoparticles inside the active layers are embedded in the PtO_x layer and are assumed to move under the influence of the readout laser beam, as shown by previous experimental work [20]. The dispersive behavior of Pt and GST is simulated by the Lorentz model [21]. The active layer (PtO_x film) is sandwiched between the insulating ZnS–SiO_2 layers and a GST-alloy phase-change data layer is located directly above this trilayer structure. The other parameters used were polarization [transverse magnetic (TM)-polarization] and cell size $\Delta = 0.5$ nm. The incident Gaussian beams with full width at half-maximum (FWHM) was adjusted such that FWHM $= 0.51\lambda/\mathrm{NA}$ [22]. The phase-change data layer is in an on-mark situation. The on-mark situation means that the incident light focuses on the recording mark. The numerical aperture of the objective lens (NA) is 0.85. As studied previously by our research group [23,24], the density of the metallic nanoparticles inside the active layer can be controlled by increasing or decreasing the incident laser power in the photodissociation process. A lower nanoparticles density shows less interaction between the nanoparticles. If the density of the nanoparticles is increased, the local-fields are coupled together and produce more evanescent fields from adjacent nanoparticles.

2. Results and discussion

Figs. 2a–d show the near-field distributions of Pt nanoparticles of normal (type A) and deformed (type B, C and D) PtO_x-type super-RENS, respectively. The total number of nanoparticles is 50 in the normal type (type A) and 58 in the deformed types (type B, C and D), each with the same diameter of 4 nm. The wavelength of incident light is $\lambda = 650$ nm for TM polarization and the refractive index of Pt is $n = 2.46 + i4.23$ [25]. In Figs. 2a–d, highly localized enhancements and interactions are produced between adjacent Pt nanoparticles in the near-field zone. When the free electrons of an Pt nanoparticle oscillate collectively in resonance with the incident light, the interaction between the incident light and Pt nanoparticles may constitute a surface plasmon polariton (SPP). The field enhancement is due to SPPs. Each embedded Pt nanoparticle behaves like a dipole and a very strong scattering center. The local-fields from adjacent nanoparticles are coupled together and produce highly enhanced evanescent fields. Since the boundary conditions of Maxwell's equations stipulate that induced surface charge density is proportional to the discontinuity of the electric field component normal to the surface, only TM-polarized light can excite SPPs.

The Pt nanoparticles inside the active layer are assumed to be under the influence of a readout incident beam. The donut shape aperture (deformed PtO_x film, i.e., type B, C and D) are formed only in the on-mark situation of the readout beam and provides the additional length (or path) longer than that of normal length (type A). In comparison with the evanescent fields for the normal type in Fig. 2a, the bubble pits of the deformed type in Figs. 2b–d give additional outer boundaries to the motion of the Pt nanoparticles, and excite more evanescent fields, which are located at the far edge (top surface) of the bubble pit from the optical axis of the incident beam. It can be clearly seen that in Figs. 2b–d that more evanescent fields extend in the direction of the propagation direction. This indicates that the bubble pit shown in Figs. 1b–d tend to increase the evanescent field intensity.

For Pt nanoparticles whose size are much smaller than the incident wavelength, their optical responses are similar to dipoles and the particle–particle interactions. As described in [26] that the local field vanishes in the gap of single pair of nanoparticles when the direction of the incident electric field is perpendicular to the major axis (light

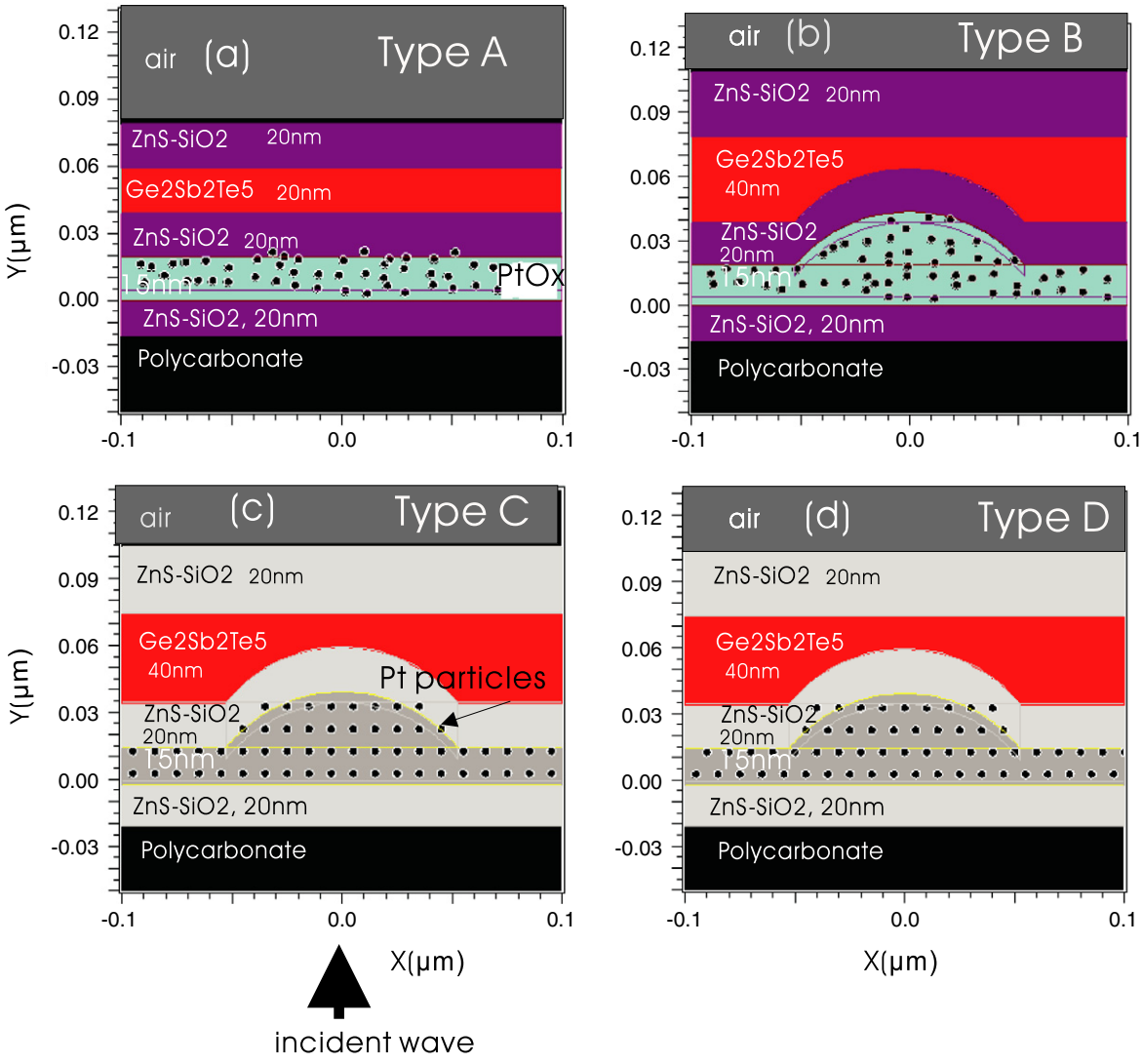

Fig. 1. Scheme of four types of pit marks formed in active layer (PtO_x film): (a) type A [normal (undeformed active layer) PtO_x-type Super RENS, Pt nanoparticles distribute in a flat active layer], (b) type B [Pt nanoparticles distributed randomly inside a bubble pit (deformed active layer)], (c) type C (Pt nanoparticles distribute in a square distribution inside the bubble pit), and (d) type D (Pt nanoparticles distribute in a triangular distribution inside the bubble pit). For these types, we assume that the Pt nanoparticles are of the same size. The layer structure is, from bottom to top, polycarbonate ($n = 1.5$)/ZnS–SiO_2($n = 2.25 + i0.01$)/PtO_x($n = 3.2 + i1.6$)/ZnS–SiO_2/$Ge_2Sb_2Te_5$ (GST, crystal phase, $n_c = 4.01 + i3.61$)/ZnS–SiO_2/air ($n = 1$).

propagation direction) of the pair. However, in a system like type A to D as shown in Figs. 1a–d (multi-pair Pt nanoparticles), the high local-field is not only confined in the gap between two Pt nanoparticles of a pair but also in the gaps between two closely spaced pairs, because of strongly pair–pair interaction. The propagation component of electric field is dominant in the gaps of the Pt nanoparticles pairs in the propagation direction, but the perpendicular component of electric field is dominant in the gaps between two closely spaced pairs. For a regular distribution system (type C and D), similar field enhancement is observed and the strongest local-field enhancement appears in the gap of Pt nanoparticle pairs. It is worthy to note that the near-field distributions of regular distribution types (Figs. 2c and d) of Pt nanoparticles in PtO_x layer are larger than that of random distribution types (Figs. 2a and b), and the out-going field emerging from the active layer (PtO_x film) in Figs. 2c and d exhibits smaller spot size than those in Figs. 2a and b. To explain this phenomenon, we can regard the regular distribution of Pt nanoparticles in active layer (type C and type D) as a plasmon waveguide [27,28]. In the waveguide energy flows from one pair of surface plasmons coupled on a pair of Pt nanoparticles to the subsequent pair excited on next pairs and so on. Difference in near-field intensity distributions of type C and type D in active layers are presented in Figs. 3a and b, respectively. The energy flows from regular distribution (type C and type D) of nanoparticle pairs can produce more surface plasmons coupled on the subsequent nanoparticle pairs. Thus, type C and type D structure can provide the direct transmission of propagation light between particle to particle. It implies that the regular distribution (type C and

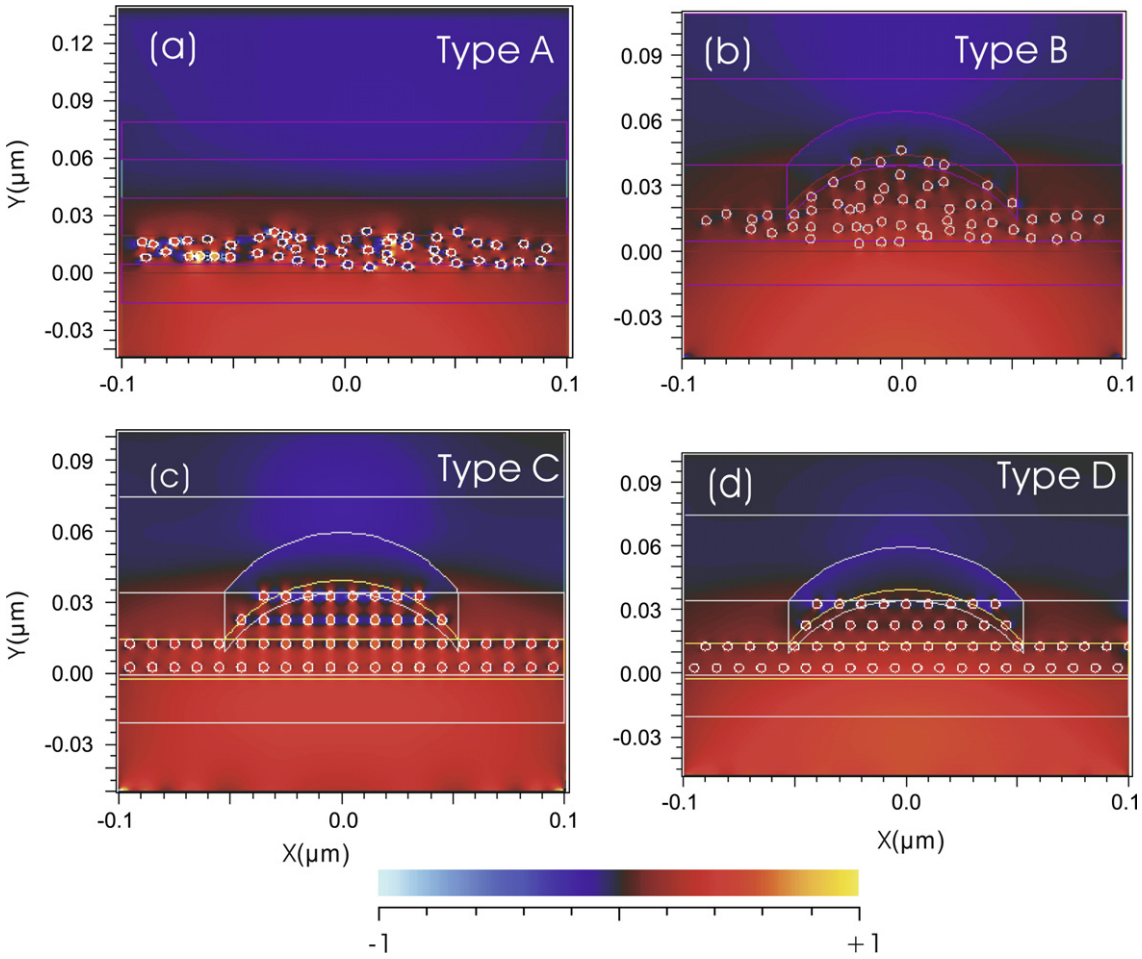

Fig. 2. The calculated results of near-field distribution of Pt nanoparticles in: (a) type A, (b) type B, (c) type C and (d) type D, respectively. The total number of nanoparticles is 50 in type A and 58 in type B, C and D, each with the same diameter of 4 nm. The wavelength of incident light is $\lambda = 650$ nm for TM polarization and the refractive index of Pt is $n = 2.46 + i4.23$.

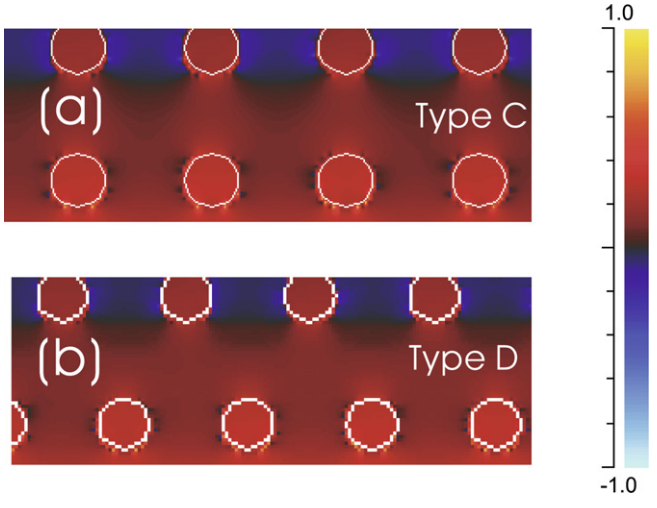

Fig. 3. Difference in near-field intensity distributions of: (a) type C and (b) type D in active layers.

type D) of Pt nonoparticles in active layer tends to be a better choice than those random distribution (type A and type B) types for the design of super-RENs near-field structure.

From experimental observation, the exact shape of a Pt nanoparticle is changed from square to circle. When the particle size increases from 3 to 11 nm, the shape becomes closer to a circle. The optical responses of Pt nanoparticles are complicated, however, one key method for understanding these effects is to distinguish the contributions from each nanoparticle and particle–particle interactions as well as the gap between two nanoparticles. SPPs and the scattering efficiency of Pt nanoparticles are usually sensitive to and controllable by particle size, the surrounding medium and the wavelength of the incident light. With the same distribution of Pt nanoparticles as shown in the Figs. 1a–d, the field intensity measured at the surface of the PtO_x layer varied considerably when they were illuminated by incident light at various frequencies (wavelengths). To verify the effect of Pt nanoparticle size, the variation in near-field intensity measured at the top surface of the active layer (PtO_x film) with increasing diameter is tested. Figs. 4 and 5 show the field intensity as a function of the diameter of Pt nanoparticles, measured at the top surface of the PtO_x film at various wavelengths of incident light. Due to the n and k values at different wavelengths of Pt and PtO_x can

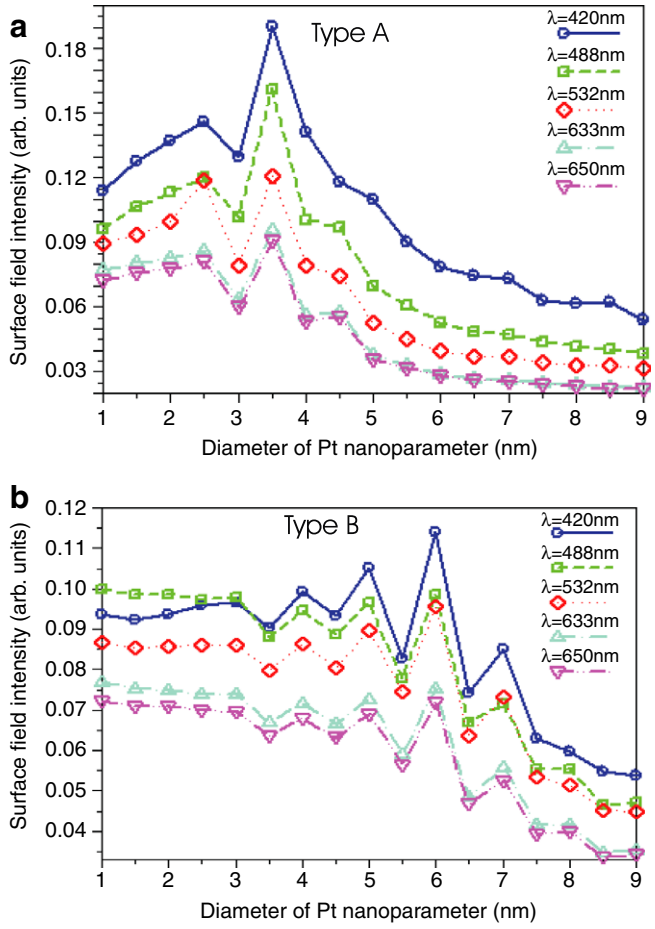

Fig. 4. The calculated results of field intensity of type A and B as a function of the diameter of Pt nanoparticles from 1 nm to 9 nm, measured at the top surface of active layer at various wavelengths of incident light.

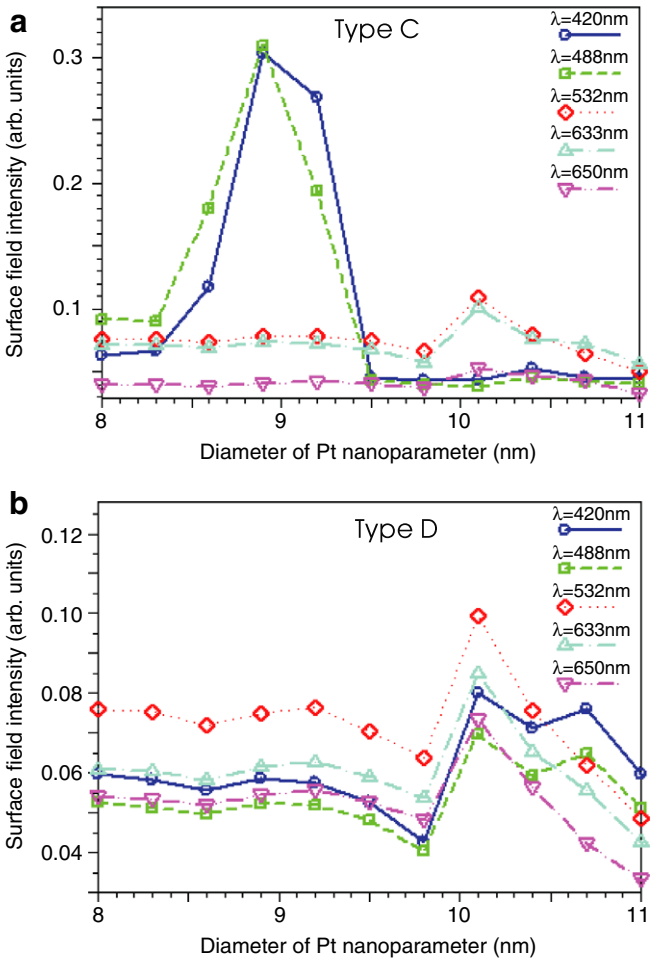

Fig. 5. The calculated results of field intensity of type C and D as a function of the diameter of Pt nanoparticles from 8 nm to 11 nm, measured at the top surface of active layer at various wavelengths of incident light.

be found in Refs. [25,29], we chose the wavelengths of incident light of 420, 488, 532, 633 and 650 nm, respectively. In the finite area of the PtO_x layer and the fixed total number of Pt nanoparticles shown in Figs. 1a–d, a smaller size of Pt nanoparticles means a lower density, because the gap between two particles is larger. In the same manner, a larger size means a higher density cases because the gap between two particles is smaller.

Figs. 4a and b show field intensity of type A and B as a function of the diameter of Pt nanoparticles from 1 nm to 9 nm, measured at the top surface of active layer at various wavelengths of incident light. The results in Figs. 4a and b show that the size variations of Pt nanoparticles may yield different field intensities and indicate that the intensities of local-fields exhibit a nonlinear optical response with increasing Pt nanoparticle diameter. It is clearly seen that the field intensity of Pt nanoparticles of the same type decreases as the wavelength of incident light increases. For type A (Fig. 4a), and type B (Fig. 4b), when Pt nanoparticle diameter was less than 1 nm, i.e., the surface area of Pt nanoparticles are too small that can excite less evanescent field from the surface, the effect of surface plasmon resonance became weaker since the evanescent light generated by smaller diameter of Pt nanoparticles which costs down the field to be transferred to propagating light. When the particle size was larger than 3.5 nm, the Pt nanoparticles in random distribution (the gaps between particle to particle are not in constant distances) that form aggregative platinum clusters which act as a platinum bulk. The intensity decreases exponentially due to the absorption in mental bulk and the destructive interference of SPPs arising from the random distribution between particle to particle interactions, while it may increase by plasmon resonance by controlling the diameter in the range of 1–3.5 nm. The field intensity at different particle diameter exhibited double peaks which were the points of surface plasmon resonance occurred, one was around 2.5 nm and the other was 3.5 nm. This indicates that the particle diameter of 2.5 nm and 3.5 nm provide a major contribution to plasmon coupling with the dipole radiation between particle to particle is the evanescent field of near-field photons. Since the field propagation is dominantly taken with the near-field photons, super-resolution exceeding the diffraction limit is made similar to that of near-field scanning optical microscopy.

The field intensity shown in Fig. 4b for type B presents a higher field intensity as the diameters of Pt nanoparticles increased in the range of 1–6 nm and then decays as the diameter larger than 6 nm (the reason why the decay of field intensity is that the gaps between nanoparticle pairs are short, and less SPPs are induced from the surface of nanoparticles). Compared to the results of type A shown in Fig. 4a, type B in Fig. 4b displays higher field intensity in a wider range (the range is nearly two times larger than that in type A) when the particle sizes are varied due to the Pt nanoparticles in the deformed active layer provides the additional length (or path) longer than the normal one (type A), and give the additional outer boundaries to the motion of the Pt nanoparticles, and also excite more evanescent field which located in the far edge of the bubble from the optical axis of the incident beam, as has discussed previously in the present paper.

Figs. 5a and b show field intensity of type C and D as a function of the diameter of Pt nanoparticles from 8 nm to 11 nm, measured at the top surface of active layer at various wavelengths of incident light. For type C and type D PtO_x-type super-RENS, it can be seen from our simulations (the results are not shown here) that the field intensity at various particle size in the range of 1–11 nm exhibits higher field intensity and the field intensity exhibits no decay in this range. This indicates that the regular distribution (i.e. type C and type D) of Pt nanoparticles in active layer is superior to the random ones (i.e. type A and type B). In Fig. 5a for type C structure, the field intensity at a fixed particle diameter exhibited peak values at shorter wavelengths (i.e. $\lambda = 420$ nm and 488 nm) at 8.9 nm and at longer wavelengths (i.e. $\lambda = 532$ nm, 633 nm and 650 nm) at 10.1 nm. In Fig. 5b for type D structure, the peak values occur at particle diameter of 10.1 nm. These were the point where surface plasmon resonance occurred. The field intensity measured at the surface of active layer of type D (see Fig. 5b) is lower than that in type C (see Fig. 5a) due to the square distribution in type C provides the direct transmission of propagation light between particle to particle, as has discussed previously in Fig. 3. It has been shown for type C that maximum value of field intensity is 0.38 (see Fig. 5a), which is nearly 1.7 times larger than the maximum value (0.19) for type A (see Fig. 4a), and also approximately 2.7 times larger than the maximum value (0.114) for type B (see Fig. 4b). It is worthy to note that the near-field distributions of regular distribution in type C and type D present no decay and promise high scattering efficiency as the particle size varied. To explain this phenomenon, the regular distribution in C and type D always exist the gaps which enhance the local-field between particle to particle. On the basis of previous simulations, we can conclude that the type C structure is the best choice in terms of higher scattering efficiency and readout stability (when the particle size varied after a writing process) in the view point of designing the PtO_x-type super-RENS.

The field pattern inside the type C of PtO_x-type super-RENS at a fixed particle diameter of 8.9 nm at wavelengths $\lambda = 420$ nm is depicted in Fig. 6. In this figure, the white and black color present the field intensity value larger (white) or lower (black) than that the maximum color used in color scale in the range of $[1, -1]$. It is clearly seen that near-field distributions show that the strongest local-field enhancement appears in the gap between particle to particle due to surface plasmon resonance. The surface plasmon resonance and light confinement of the square distribution of Pt nanoparticles can be tuned by diameter of Pt nanoparticles, interpair distance, and the wavelength of incident light.

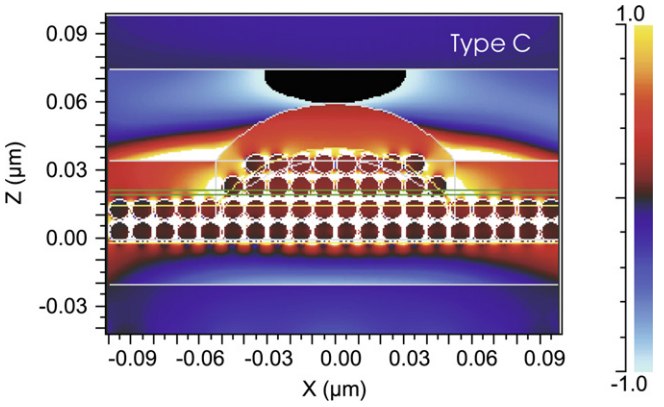

Fig. 6. The field pattern inside the type C of PtO_x-type super-RENS at a fixed particle diameter of 8.9 nm at wavelength $\lambda = 420$ nm.

The nano-size Pt particles are embedded in the PtO_x layer either by the fabrication process or by the photo dissociation process with incident laser light, and one can control the distribution of Pt nonoparticles and tend to the square distribution inside the active layer by adjusting the power of incident laser power as observed in our recent experiments [30]. If such a spatial distribution of materials within the super-RENS active layer that produces the desired results are able to find, it would enable us to model the super-RENS writing and reading process and to better understand the super-RENS phenomenon. In addition, by manipulating the localized surface plasmon resonance, local-field enhancement, and near-field coupling of nanoparticles, it is promising to be able to focus, to transport, and to interact with light in nano-scale region and are being explored for various applications in chemical biological sensors [31], and nano photonic device.

In further research, we will consider the model where not a single bubble pit but two or more pits are in one spot. Moreover, on the basis of results of this study, we will calculate the change in intensity (difference signal) in the far-field by varying mark size, the distribution, and the number of metallic particles in the active layer that become detectable signals.

3. Conclusion

In conclusion, the distribution and plasmon effects of collective localized surface plasmons between incident light

and active layer of PtO_x-type super-RENS have been studied using finite-difference time-domain method. Four types of distribution of Pt nanoparticles in active layer are investigated. We find that the regular distribution of Pt nanoparticles in active layer can provide higher field intensity in a wider range of particle size when the particle sizes are varied, and the out-going filed emerging from the active layer exhibit smaller spot size than that of random arrangement one. The deformed type of Pt nanoparticles PtO_x-type super-RENS provides the additional length (or path) longer than that of the normal one and give the additional outer boundaries to the motion of the Pt nanoparticles, and excite more evanescent field which located in the far edge of the bubble from the optical axis of the incident beam. On the basis of simulations, we can conclude that the type C structure is the best choice in terms of higher scattering efficiency and readout stability in the view point of designing the PtO_x-type super-RENS. Our results provide new information to design a super-RENS with superior resolution as well as an alternative approach to near-field optical research, plasmon device, biological sensors and nano photonic devices.

Acknowledgements

The authors are thankful for the financial support from the National Science Council, Taiwan, ROC, under Grant Number NSC 96-2112-M-231-001-MY3 and NSC96-2120-M-002-017.

References

[1] W.C. Liu, C.Y. Wen, K.H. Chen, W.C. Lin, D.P. Tsai, Appl. Phys. Lett. 78 (2001) 685.
[2] H. Fuji, J. Tominaga, L. Men, T. Nakano, H. Katayama, N. Atado, Jpn. J. Appl. Phys. 39 (2000) 980.
[3] J. Tominaga, T. Nakano, N. Atoda, Appl. Phys. Lett. 73 (1998) 2078.
[4] J. Tominaga, T. Nakano, N. Atoda, Proc. SPIE 3467 (1998) 282.
[5] J. Tominaga, H. Fuji, A. Sato, T. Nakano, T. Fukaya, N. Atoda, Jpn. J. Appl. Phys. 37 (1998) L1323.
[6] T. Nakano, A. Sato, H. Fuji, J. Tominaga, N. Atoda, Appl. Phys. Lett. 75 (1999) 151.
[7] T. Fukaya, J. Tominaga, T. Nakano, N. Atoda, Appl. Phys. Lett. 75 (1999) 3114.
[8] T. Kikukawa, N. Fukuzawa, T. Kobayashi, Jpn. J. Appl. Phys. 44 (2005) 3596.
[9] J. Kim, I. Hwang, H. Kim, I. Park, J. Tominaga, Jpn. J. Appl. Phys. 44 (2005) 3609.
[10] T. Kikukawa, T. Nakano, T. Shima, J. Tominaga, Appl. Phys. Lett. 81 (2002) 4697.
[11] K. Kurihara, T. Arai, T. Nakano, J. Tominaga, Jpn. J. Appl. Phys. 44 (2005) 3353.
[12] T.C. Chu, W.C. Liu, D.P. Tsai, Opt. Commum. 246 (2005) 561.
[13] W.C. Liu, M.Y. Ng, D.P. Tsai, Jpn. J. Appl. Phys. 43 (2004) 4713.
[14] W.C. Liu, D.P. Tsai, Jpn. J. Appl. Phys. 42 (2003) 2078.
[15] M.Y. Ng, W.C. Liu, Opt. Exp. 14 (2005) 9422.
[16] T. Na, Y. Yamakawa, J. Tominaga, N. Atoda, Jpn. J. Appl. Phys. 40 (2001) 1531.
[17] T. Kikukawa, A. Tachibana, H. Fuji, J. Tominaga, Jpn. J. Appl. Phys. 42 (2003) 1038.
[18] H. Fuji, T. Kikukawa, J. Tominaga, Jpn. J. Appl. Phys. 43 (2004) 4212.
[19] A. Taflove, Computational Electrodynamics: The Finite-Difference Time-Domain Method, second ed., Artech House, Norwood, MA, 2000.
[20] B.S. Lin, D.P. Tsai, W.C. Lin, ISOM Tech. Dig., 2003, Th-H-02.
[21] J.B. Judkins, R.W. Ziolkowski, J. Opt. Soc. Am. A12 (1995) 974.
[22] S.G. Stan, The CD-ROM Drive; A Brief System Description, Kluwer Academic, Boston, 1998, p. 16, (Chapter. 2.3).
[23] W.-C. Liu, D.P. Tsai, Jpn. J. Appl. Phys. 42 (2003) 1031.
[24] T.-C. Chu, W.-C. Liu, D.P. Tsai, Scanning 26 (2004) I-102.
[25] Chian Liu, J. Erdmann, J. Maj, A. Macrander, J. Vac. Sci. Technol. A 17 (5) (1999) 2741.
[26] J. Kottmann, O. Martin, Opt. Exp. 8 (2001) 655.
[27] M.Y. Ng, W.C. Liu, Opt. Exp. 14 (2006) 505.
[28] W.M. Saj, Opt. Exp. 13 (2005) 4818.
[29] T. Shima, J. Tominaga, Jpn. J. Appl. Phys. 42 (2003) 3476.
[30] F.H. Ho, H.H. Chang, Y.H. Lin, B.-M. Chen, S.-Y. Wang, D.P. Tsai, Jpn. J. Appl. Phys. 42 (2003) 1000.
[31] D.A. Schultz, Curr. Opin. Biotechnol. 14 (2003) 13.